Contrib Mineral Petrol
DOI 10.1007/s00410-012-0769-x

ORIGINAL PAPER

Redox-controlled iron isotope fractionation during magmatic differentiation: an example from the Red Hill intrusion, S. Tasmania

Paolo A. Sossi · John D. Foden · Galen P. Halverson

Received: 13 November 2011 / Accepted: 14 May 2012

Abstract This study presents accurate and precise iron isotopic data for 16 co-magmatic rocks and 6 pyroxene–magnetite pairs from the classic, tholeiitic Red Hill sill in southern Tasmania. The intrusion exhibits a vertical continuum of compositions created by in situ fractional crystallisation of a single injection of magma in a closed igneous system and, as such, constitutes a natural laboratory amenable to determining the causes of Fe isotope fractionation in magmatic rocks. Early fractionation of pyroxenes and plagioclase, under conditions closed to oxygen exchange, gives rise to an iron enrichment trend and an increase in f_{O_2} of the melt relative to the Fayalite–Magnetite–Quartz (FMQ) buffer. Enrichment in $Fe^{3+}/\Sigma Fe_{melt}$ is mirrored by $\delta^{57}Fe$, where $^{VI}Fe^{2+}$-bearing pyroxenes partition ^{57}Fe-depleted iron, defining an equilibrium pyroxene-melt fractionation factor of $\Delta^{57}Fe_{px-melt} \leq -0.25\,‰ \times 10^6/T^2$. Upon magnetite saturation, the f_{O_2} and $\delta^{57}Fe$ of the melt fall, commensurate with the sequestration of the oxidised, ^{57}Fe-enriched iron into magnetite, quantified as $\Delta^{57}Fe_{mtn-melt} = +0.20\,‰ \times 10^6/T^2$. Pyroxene–magnetite pairs reveal an equilibrium fractionation factor of $\Delta^{57}Fe_{mtn-px} \approx +0.30\,‰$ at 900–1,000 °C. Iron isotopes in differentiated magmas suggest that they may act as an indicator of their oxidation state and tectonic setting.

Keywords Iron isotopes · Tholeiitic differentiation · Fractional crystallisation · Oxygen fugacity · Tasmanian Dolerites · High-temperature stable isotopes

Communicated by F. Poitrasson.

Electronic supplementary material The online version of this article (doi:10.1007/s00410-012-0769-x) contains supplementary material, which is available to authorized users.

P. A. Sossi · J. D. Foden
School of Earth and Environmental Sciences,
University of Adelaide, Adelaide, SA 5000, Australia

P. A. Sossi (✉)
Research School of Earth Sciences, Australian National University, Canberra, ACT 0200, Australia
e-mail: paolo.sossi@anu.edu.au

G. P. Halverson
Department of Earth and Planetary Sciences,
McGill University, 3450 University Street,
Montreal, QC H3A 2A7, Canada

Introduction

Since iron is the most abundant polyvalent species in silicate melts, the relative proportion of ferrous to ferric iron control the oxygen fugacity (f_{O_2}) of the liquid (e.g. Jayasuriya et al. 2004):

$$Fe^{2+}O + \frac{1}{4}O_2 = Fe^{3+}O_{1.5} \quad (1)$$

Changing f_{O_2} effects a commensurate change in the stability of mineral phases that incorporate ferrous and ferric iron, thereby controlling the liquid line of descent of magmas undergoing differentiation. For example, increasing f_{O_2} favours magnetite crystallisation while increasing the Mg# of co-existing Fe–Mg silicates (Snyder et al. 1993; Toplis and Carroll 1995; Berndt et al. 2005; Botcharnikov et al. 2008; Feig et al. 2010).

Two iron-bearing phases pivotal to both magma series, olivine and magnetite, were equilibrated with quartz, forming the buffer assemblage, fayalite–magnetite–Quartz (FMQ), and the ensuing iron isotope fractionation between them, at equilibrium, was measured by Shahar et al. (2008).

Published online: 06 June 2012

Their results reveal a systematic enrichment in ^{57}Fe in magnetite with respect to fayalite, expressed as:

$$\Delta^{57}Fe_{mtn-fay} = +0.30 \pm 0.024\,‰ \times 10^6/T^2 \quad (2)$$

where the fractionation factor is given by $\Delta^{57}Fe_{A-B} = \delta^{57}Fe_A - \delta^{57}Fe_B$. These systematics are in agreement with theoretical mechanics for equilibrium stable isotope fractionation (e.g. Schauble 2004), which predict higher β-factors for minerals with higher $Fe^{3+}/\Sigma Fe$. This behaviour reflects the greater charge density of oxidised species, which tend to exist in lower co-ordination polyhedra (IV-fold rather than VI-fold), forming shorter (and thus stiffer) bonds. The stiffer bonds preferentially incorporate the heavier isotope in aid of minimising the vibrational energy associated with the bond. The isotopic composition of iron in a given phase is expected to scale with its mean co-ordination number, which is often dependent on its oxidation state.

Corroboration of these isotope-partitioning mechanics at high temperatures comes from a series of studies on natural magmas. Contrary to earlier reconnaissance studies (Beard et al. 2003), investigations of specific suites of magmatic rocks provide evidence for the isotopic fractionation of iron during differentiation. $\delta^{57}Fe$ ($\delta^{57}Fe = (^{57/54}Fe_{smp}/^{57/54}Fe_{std} - 1) \times 1{,}000$) displays a monotonic increase with decreasing MgO at the Kilauea Iki lava lake, Hawai'i, which Teng et al. (2008) attributed to the removal of olivine that contains exclusively ferrous iron, and is correspondingly ^{57}Fe-depleted. Silicic differentiates of the Hekla volcanic suite, Iceland, also display a tendency to evolve towards more ^{57}Fe-enriched compositions (Schuessler et al. 2009). Such trends are not restricted to volcanic rocks; Poitrasson and Freydier (2005) report isotopic compositions of granitoids up to $\delta^{57}Fe = +0.58$ ‰, a change ascribed to the exsolution of reduced, Fe^{2+}-bearing and, consequently, ^{57}Fe-depleted fluids. This model was supported by Heimann et al. (2008), citing a large fractionation factor between magnetite and fluid, $\Delta^{57}Fe_{mtn-Fe^{2+}fluid} \approx +0.42\,‰ \times 10^6/T^2$. The relative constancy of monovalent isotopes such as Li and Mg during these processes (Tomascak et al. 1999; Teng et al. 2007) suggests that the driver for isotopic fractionation is endemic to Fe. These considerations indicate that the fractionation at high temperatures is linked to changes in the redox state of iron.

The complexity of natural systems blurs the processes that engender iron isotope fractionation, such that systematic investigations are required to address the nature of these processes. The Red Hill intrusion, southern Tasmania (Fig. 1), is ideal for this study. By utilising a series of natural samples that record the progressive differentiation of a single batch of tholeiitic magma by fractional crystallisation (McDougall 1962), it enables quantification of fractionation factors between igneous minerals and melt. The carapace of chilled dolerite, which lines the margins of intrusion, not only represents a clear parent magma composition from which to model the observed fractionation, but also acted to shield the evolving magma from interaction with adjacent country rocks during its differentiation. Thus, the magma evolved as a system closed with respect to oxygen, resembling a natural laboratory.

The aim of this work is to present evidence for the differences in iron isotope composition between ferrous and ferric iron phases and their impact on the iron isotope composition of the evolving melt. As the f_{O_2} of the melt exerts a dominant control on its $Fe^{3+}/\Sigma Fe$ and, in turn, on the phases that form, the iron isotope signature of an igneous rock should record the redox conditions of its crystallisation. We show that crystallisation of Fe^{2+}-bearing pyroxenes partitions ^{57}Fe-depleted iron, causing the f_{O_2} and $\delta^{57}Fe$ of the melt to increase. The resultant increase in Fe^{3+} (and therefore f_{O_2}) in the residual melt triggers magnetite saturation, which sequesters isotopically heavy iron, leaving the melt with a ^{57}Fe-depleted composition. These $\delta^{57}Fe$-f_{O_2} systematics are applied to distinguish magmas with different oxidation states (calc-alkaline vs. tholeiitic) and, similarly, different tectonic settings (anorogenic A-Type vs. collisional I-type granites).

Background and samples

The Red Hill intrusion comprises a section of the voluminous Tasmanian Dolerites, which represent the northernmost extent of magmatism associated with the Ferrar Large Igneous Province, a linear belt of tholeiitic magma emplaced along the footprint of the Cambro-Ordovician Delamerian-Ross Orogen (Foden et al. 2006) in a short pulse at ca. 180 Ma (Schmidt and McDougall 1977; Encarnaciòn et al. 1996; Williams and Hergt 2000).

The chilled margins of the intrusion are composed of a fine groundmass of plagioclase (45 %), three pyroxenes (55 %) and accessory ilmenite. Orthopyroxene, En_{83}, occurs as homogeneous microphenocrysts and is limited to the chilled dolerites (Fig. 2a; Hergt et al. 1989).

Further from the margins, dolerites and quartz dolerites occupy the lower $\approx$200 m of the $\approx$420-m-thick intrusion (Fig. 3) and are typified by augite(25 %)–pigeonite(20 %)–plagioclase(55 %) assemblages, where cumulophyric pyroxene clusters partially envelop plagioclase crystals, defining a sub-ophitic texture. Pigeonite and augite are extensively normally zoned in Fe–Mg, with a single grain showing variation in Mg# ($Mg/(Mg + \Sigma Fe)$) from 75 in the core to 30 in the rim (Fig. 2b). Intercumulus ulvöspinel-rich titanomagnetite (Mtn_{40}–Mtn_{70}) joins ilmenite as the crystallising oxides.

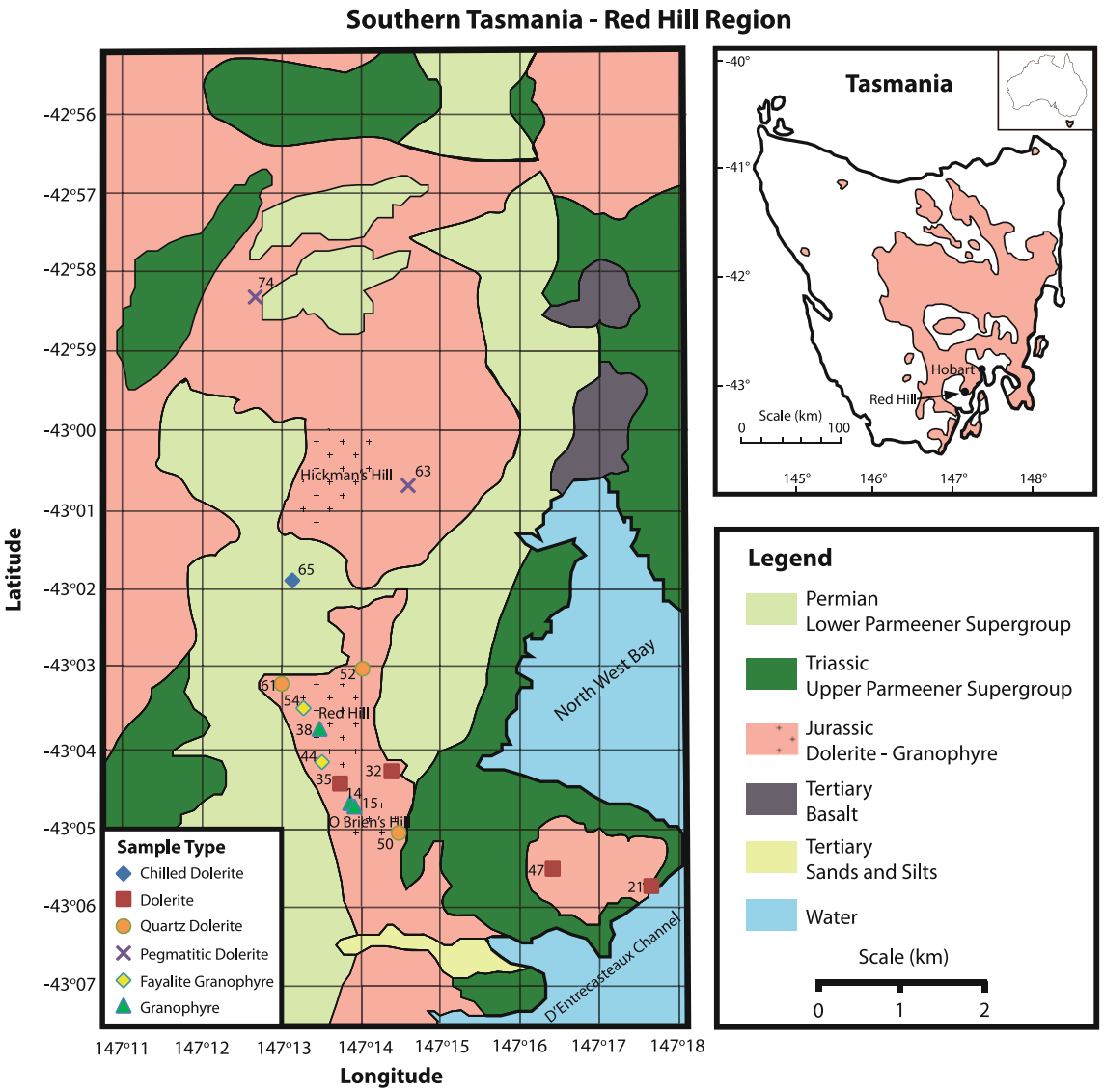

Fig. 1 Geological map of the Red Hill region of southern Tasmania. Sample locations and rock type are also shown. The dolerite (*pink*) forms a sheet-like sill and is capped by granophyric rocks, which occupy cupolas that uplifted the roof rocks and now form hills in the area (*crosses*)

The extended, normal core-rim Fe–Mg pyroxene zonation ceases upon the crystallisation of cumulus magnetite (15 %, Mtn_{95}) and fayalite (<5 %, Fa_{95}) in the fayalite granophyres, marking the transition between dolerites and granophyres (Fig. 3). Clinopyroxene constitutes a diminishing proportion of the assemblage (10 %), occurring as unzoned brown ferroaugite ($Di_{30–20}$), commonly rimmed by vermicular hedenbergite ($Di_{15–10}$) (Fig. 2c). A sodic plagioclase–K–feldspar–quartz groundmass comprises the bulk of the rock, nearing 70 %).

Granophyric quartz-K-feldspar intergrowths comprise ≈50 % of the most differentiated granophyres, which contain only clinopyroxene (5 %, hedenbergite) and magnetite (20 %) as their iron-bearing phases (Fig. 2d). Separate sodic plagioclase, K-feldspar and quartz crystals comprise the remaining 25 % of the rock, which are invariably present at the highest stratigraphic levels, occupying 'cupola' structures which now form hills in the area (McDougall 1962).

The whole rocks define coherent trends in an alkali–iron–magnesia (AFM) diagram (Fig. 4a), preserving aliquots of the liquid's composition at different stages of its fractionation history. Initial segregation of pyroxenes and plagioclase results in iron enrichment without an appreciable increase in SiO_2 content. Conversely, following magnetite saturation, SiO_2 drastically increases, whereas ΣFe falls dramatically, with a concomitant increase in alkalis. Such an evolution is expected of liquids with low

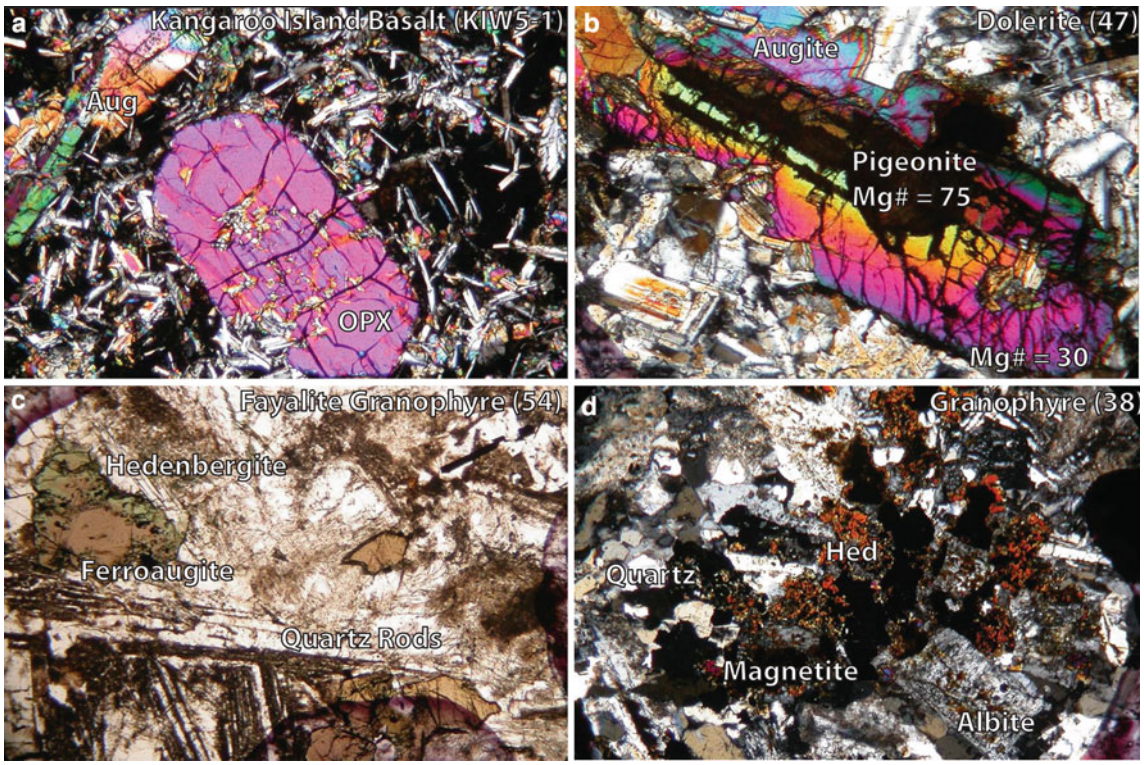

Fig. 2 Photomicrographs of representative samples of the Red Hill intrusion. **a** Euhedral orthopyroxene microphenocryst in a Kangaroo Island Basalt (KIW5-1). **b** Extensive, normal Fe–Mg zonation in a pigeonite from dolerite 47. **c** Fayalite granophyre (54) typified by brown augite rimmed by green hedenbergite. **d** Differentiated granophyre (38), with an association of magnetite, hedenbergite, quartz and alkali feldspars. Field of view is 2 mm in all cases

f_{O_2} (delaying magnetite) and low $a_{H_2O}^{liquid}$ (stabilising plagioclase), resulting in the development of a tholeiitic trend (e.g. Toplis and Carroll 1995; Botcharnikov et al. 2008).

The 16 samples investigated in this study encapsulate the complete range of chemical variation in the Red Hill intrusion (Table 1; Fig. 4a). These samples come from a limited geographical area and show geochemical trends which suggest they were produced from closed-system crystal fractionation of a single parent magma, represented by the chilled dolerites. In addition, in order to characterise intermineral fractionation and facilitate comparison with whole rocks, pyroxene separates were analysed for 7 of these rocks, and magnetite for 6. Analysis of mineral pairs enables an assessment of the extent of equilibrium achieved and whether kinetic effects (e.g. diffusive disequilibrium) have affected their isotopic composition.

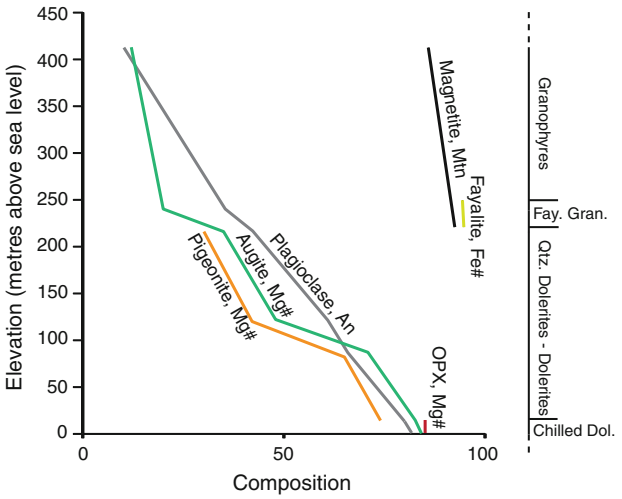

Fig. 3 Compositional variation in the Red Hill intrusion as illustrated by the mineral crystallisation sequence and chemistry. Composition corresponds to Mg# (orthopyroxene, pigeonite, augite), anorthite content (plagioclase), Fe# (fayalite) and magnetite content (magnetite)

Analytical techniques

MC-ICP-MS

Samples were dissolved in a concentrated HF–HNO_3–HCl solution before being passed through anion exchange columns (AG1-X4, 200–400 mesh) in chloride form to ensure quantitative separation of iron from similar matrix elements (Poitrasson and Freydier 2005). Fe solutions of 4 ppm (H-cones) and 1.5 ppm (X-cones) were run on a ThermoFinnigan Neptune Multicollector ICP-MS (CSIRO,

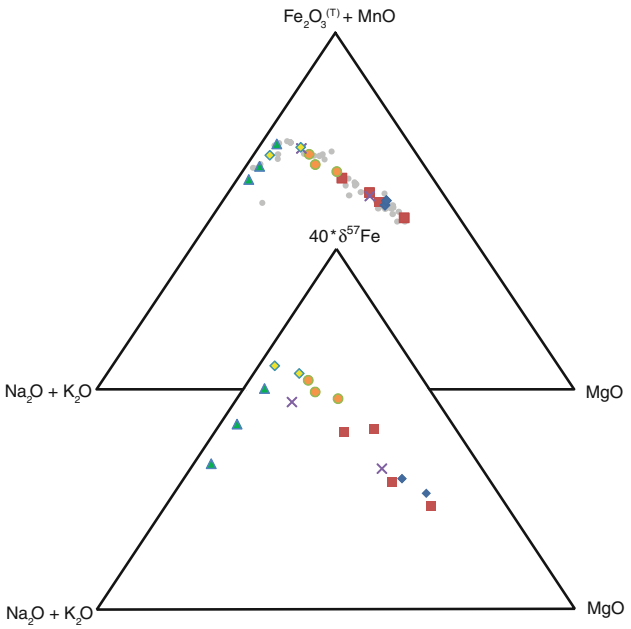

Fig. 4 Ternary Alkalis $Fe_2O_3^{(T)}$ + MnO–MgO (AFM) diagram illustrating the tholeiitic evolution shown by the Red Hill magmas (*grey dots* represent the entire chemical variation in the suite). Substituting 40× δ^{57}Fe for $Fe_2O_3^{(T)}$ + MnO results in the same broad trend, suggesting that these two quantities are linked (see "Petrologic evolution of the Red Hill Suite"). *Symbols* as per Fig. 1

University of Adelaide, Waite Campus) in solution mode with a glass spray chamber and Scott double-pass assembly coupled to a low-flow PFA Nebuliser sample introduction mechanism. The resulting sensitivity was 6.5 V ^{56}Fe/ppm (H) and 17 V ^{56}Fe/ppm (X). Magnetite and pyroxene data were acquired on a Neptune Plus housed at the Australian National University, using an identical set-up. Data quality control was assured through the continual running of the hematite internal standard (ETH, Zürich), in addition to running processed BHVO-2 and BCR-2, and re-running two separate dissolutions of three samples on both the Adelaide and ANU Neptune. Data are corrected using the Ni-spiking regime of Poitrasson and Freydier (2005), resulting in external precision of better than ±0.03 ‰ for δ^{56}Fe and ±0.05 ‰ for δ^{57}Fe, providing ^{61}Ni ≈ 1 V. All data are reported relative to the international isotopic reference standard IRMM-014 (Taylor et al. 1992).

FeO determinations

The ferrous iron content of the whole rocks was determined by volumetric wet chemical analysis, as developed by Wilson (1960). The procedure relies upon the quantitative oxidation of Fe^{2+} in the sample by V^{5+}, as the V^{4+} produced is more resistant to accidental oxidation during hot acid dissolution (48 % HF-9 M H_2SO_4) than is ferrous

Table 1 XRF major element data (wt%) for all samples investigated

Sample	Type	SiO_2	Al_2O_3	$Fe_2O_3^{(T)}$	FeO	MnO	MgO	CaO	Na_2O	K_2O	TiO_2	P_2O_5	SO_3	LOI	$Fe^{3+}/\Sigma Fe$	Total	Temperature (°C) (S + G, 1993); ±7 °C
KIW5-1	KI Basalt	53.89	14.52	10.43	7.5	0.18	6.86	10.69	1.83	0.73	0.65	0.11	0.03	0.12	0.20	100.04	1,179
65	Chilled Margin	54.17	14.63	9.96	7.6	0.17	6.77	10.79	1.84	0.84	0.64	0.11	0.02	0.00	0.15	99.94	1,183
47	Dolerite	54.28	14.49	10.49	6.8	0.17	5.69	10.18	2.00	0.92	0.71	0.12	0.02	0.89	0.25	99.96	1,145
50	Qtz. Dolerite	56.13	15.67	11.70	7.5	0.16	2.08	8.06	2.59	1.47	1.12	0.16	0.03	1.00	0.29	100.17	1,103
35	Dolerite	53.39	17.51	9.70	7.6	0.15	3.61	10.52	2.20	0.96	0.70	0.12	0.02	0.83	0.13	99.71	1,157
54	Fay. Granophyre	61.31	13.15	13.02	6.1	0.14	0.60	5.05	2.91	2.40	0.93	0.26	0.03	1.56	0.48	101.36	1,003
38	Granophyre	62.54	10.84	12.84	5.6	0.16	0.62	3.99	2.61	2.64	1.15	0.35	0.01	1.39	0.52	99.14	980
14	Granophyre	64.32	11.81	10.02	5.3	0.14	0.47	3.84	2.84	2.77	0.91	0.23	0.02	2.06	0.42	99.43	957
15	Granophyre	66.17	12.15	8.83	5.4	0.12	0.38	3.14	3.08	2.80	0.93	0.24	0.01	1.60	0.33	99.45	961
63	Peg. Dolerite	59.65	11.91	13.42	7.8	0.17	1.83	5.50	2.63	2.04	1.37	0.22	0.02	1.05	0.35	99.81	1,048
44	Qtz. Dol.–Fay Gran.	56.62	15.21	12.30	5.3	0.15	1.61	7.05	2.64	1.63	1.38	0.17	0.01	1.38	0.53	100.15	1,074
61	Qtz. Dol.–Fay Gran.	56.00	15.71	11.15	6.4	0.16	2.54	8.32	2.65	1.41	0.95	0.16	0.02	0.79	0.36	99.86	1,116
21	Dolerite	54.63	14.41	10.20	7.3	0.17	6.29	10.22	2.04	0.91	0.66	0.12	0.02	0.32	0.20	99.99	1,164
52	Qtz. Dolerite	54.65	15.98	10.68	7.8	0.16	3.50	9.57	2.27	1.12	0.83	0.14	0.02	0.84	0.19	99.76	1,138
32	Dolerite	53.13	15.00	9.06	7.0	0.16	7.72	11.98	1.57	0.63	0.51	0.10	0.02	0.12	0.14	100.00	1,194
74	Peg. Dolerite	55.56	13.71	10.62	5.2	0.18	5.99	9.61	2.05	1.09	0.74	0.13	0.01	0.46	0.46	100.15	1,148

iron. Ferrous iron is regenerated by back-titration with ammonium ferrous sulphate, from which the original Fe^{2+} content may be calculated. The procedural uncertainties are on the order of ±0.1 wt % FeO.

A more detailed treatment for both methods may be accessed in Online Resources A and B, respectively.

Results

Whole-rock isotopic compositions measured ($\delta^{57}Fe = +0.12 \pm 0.06$ ‰ to $+0.31 \pm 0.03$ ‰; 2SE, Table 2) span the range reported for terrestrial igneous rocks (Poitrasson and Freydier 2005; Schoenberg and von Blanckenburg 2006; Dauphas et al. 2009).

Whole-rock $\delta^{57}Fe$ shows well-defined trends against MgO, an index of igneous differentiation (Fig. 5a). Initially, $\delta^{57}Fe$ displays a systematic increase with falling MgO, similar to that observed at Kilauea Iki (Teng et al. 2008). A notable feature is the abrupt decrease in $\delta^{57}Fe$ below ≈1 wt% MgO, a point coincident with the rapid depletion of $Fe_2O_3^{(T)}$. Samples at the apex of this trend are the fayalite granophyres, which have both the highest concentration of iron (≈13 wt%, Fe as $Fe_2O_3^{(T)}$; Table 1) and the most ^{57}Fe-enriched compositions (up to $\delta^{57}Fe = +0.31$ ‰; Table 2). Consequently, $\delta^{57}Fe$ of the whole rocks preserve a positive linear correlation with their iron contents (Fig. 5b) throughout the entire differentiation sequence.

Over the same MgO interval, the $Fe^{3+}/\Sigma Fe$ increases proportionally with $\delta^{57}Fe$, prior to reaching an inflection point, after which the residual liquid is depleted in both Fe^{3+} and ^{57}Fe (Fig. 5c). Thus, the evolution of iron in the liquid is controlled first by fractionation of a Fe^{3+}-poor, ^{57}Fe-poor phase, which increases the f_{O_2} of the melt, before becoming saturated in a Fe^{3+}-rich, ^{57}Fe-rich phase, which drives the composition of the liquid in the opposite direction.

Table 2 Iron isotope data for all samples investigated expressed in per mille (‰) and their associated uncertainties (2 standard error)

Sample	Type	$\delta^{57}Fe$	±(2SE)	$\delta^{56}Fe$	±(2SE)	Repetitions
KIW5-1	K.I. Basalt	0.145	0.031	0.101	0.029	4
65	Chilled Margin	0.134	0.020	0.082	0.061	3
65-PX		0.110	0.028	0.078	0.020	4
47	Dolerite	0.216	0.023	0.153	0.014	3
47-PX		−0.168	0.025	−0.105	0.007	4
47-Mtn		0.604	0.055	0.423	0.028	5
50	Qtz. Dolerite	0.267	0.025	0.195	0.011	4
50-PX		−0.041	0.045	−0.028	0.012	3
50-Mtn		0.467	0.010	0.294	0.056	3
35	Dolerite	0.163	0.027	0.120	0.035	4
54	Fay. Granophyre	0.307	0.030	0.196	0.028	3
54-PX		0.071	0.034	0.048	0.020	4
54-Mtn		0.360	0.039	0.253	0.044	5
38	Granophyre	0.226	0.024	0.147	0.024	4
38-PX		−0.118	0.039	−0.078	0.019	4
38-Mtn		0.208	0.020	0.154	0.034	3
14	Granophyre	0.157	0.033	0.101	0.020	6
14-PX		−0.186	0.006	−0.126	0.012	3
14-Mtn		0.165	0.029	0.103	0.021	4
15	Granophyre	0.105	0.056	0.070	0.045	5
15-PX		−0.201	0.007	−0.140	0.008	3
15-Mtn		0.109	0.021	0.069	0.019	3
63	Peg. Dolerite	0.219	0.031	0.139	0.026	4
44	Qtz. Dol.–Fay. Gran.	0.278	0.050	0.186	0.035	5
61	Qtz. Dol.–Fay. Gran.	0.251	0.063	0.184	0.054	3
21	Dolerite	0.126	0.037	0.087	0.030	7
52	Qtz. Dolerite	0.240	0.033	0.161	0.026	3
32	Dolerite	0.117	0.058	0.084	0.040	3
74	Peg. Dolerite	0.145	0.048	0.096	0.035	3
BHVO-2	Hawaiian Basalt	0.159	0.068	0.104	0.043	4
BCR-2	Columbia River Basalt	0.139	0.044	0.091	0.034	4
HEM	Haematite (ETH)	0.760	0.026	0.513	0.022	16

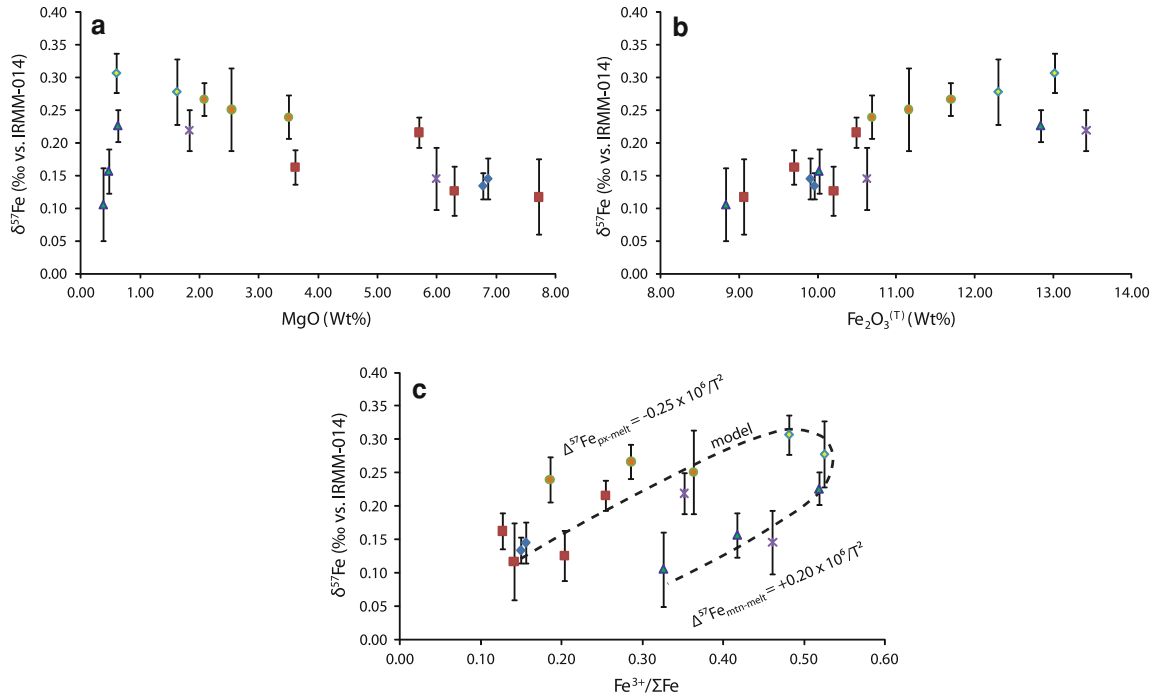

Fig. 5 Variation of measured whole-rock δ^{57}Fe with other compositional parameters; **a** MgO, **b** $Fe_2O_3^{(T)}$, **c** $Fe^{3+}/\Sigma Fe$. The Rayleigh model (*dashed line*) assumes that $\Delta^{57}Fe_{px-melt} = -0.25\,‰ \times 10^6/T^2$ and that $\Delta^{57}Fe_{mtn-melt} = +0.20‰ \times 10^6/T^2$. All error bars are absolute 2σ. Symbols as per Fig. 1

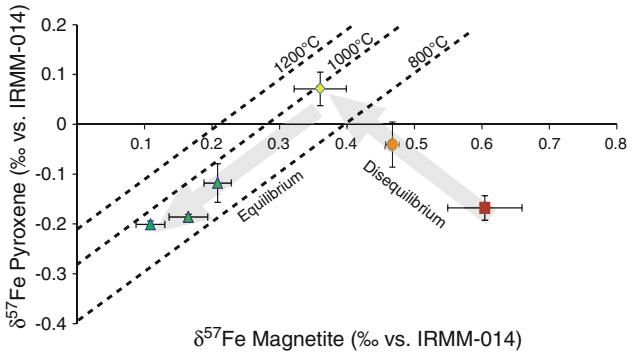

Fig. 6 Comparison of $\delta^{57}Fe_{px}$ to $\delta^{57}Fe_{mtn}$, where the fractionation factor is given by subtracting one value from the other. *Dashed lines* are expected equilibrium iron isotope fractionation factors calculated from Polyakov and Mineev (2000) and Polyakov et al. (2007). Symbols as per Fig. 1

Pyroxene–magnetite data are displayed graphically in Fig. 6. Pyroxenes in the chilled dolerites ($\delta^{57}Fe = +0.11 \pm 0.028$ ‰) have a composition indistinguishable from that of the whole rock ($+0.13 \pm 0.02$ ‰), which is expected given that they host the bulk of the Fe. More unexpected, however, is the light δ^{57}Fe of the pyroxenes in the dolerites and quartz dolerites ($\delta^{57}Fe = -0.17$, and -0.10 ‰, respectively), and the correspondingly heavy titanomagnetite compositions of $+0.60$ and $+0.46$ ‰. The first appearance of cumulus magnetite in the fayalite granophyres has $\delta^{57}Fe = +0.36$ ‰, slightly heavier than its whole rock ($+0.31$ ‰) and coexisting pyroxene ($+0.07$ ‰), defining a $\Delta^{57}Fe_{mtn-px} = +0.29\,‰$. The more differentiated granophyres have magnetite whose δ^{57}Fe cluster near to the whole-rock value, while the pyroxenes are considerably lighter, resulting in a constant $\Delta^{57}Fe_{mtn-px} \approx +0.32\,‰$.

Discussion

Petrologic evolution of the Red Hill suite

Superficially, the trend defined by the whole rocks in δ^{57}Fe–MgO (Fig. 5a) space resembles that of an evolving tholeiitic magma in an AFM diagram (Fig. 4b). This similarity suggests that the process responsible for the variation in the total iron content of the magma also controls its iron isotopic composition. It has been demonstrated experimentally, and confirmed in natural magmas, that the tholeiitic trend arises due to fractional crystallisation of a silica-rich basaltic liquid with low $f_{O_2}, a_{H_2O}^{liquid}$ at relatively low pressures (Fenner 1929; Osborn 1959; Toplis and Carroll 1995; Botcharnikov et al. 2008). The distinguishing feature of tholeiitic differentiation is the initial increase in total iron content of the magma, prior to its depletion at a late stage in its evolution.

Typical tholeiitic differentiation is controlled first by the fractionation of pyroxenes and plagioclase, before

magnetite becomes the dominant iron-bearing phase (Campbell and Nolan 1974). This order of crystallisation is also observed at Red Hill (Fig. 3). Iron can be described in terms of ferrous and ferric iron, both of which are present in magmas in the range of terrestrial oxygen fugacities (Papike et al. 2005). Ferrous iron tends to partition into olivine and pyroxenes, while ferric iron only becomes compatible when magnetite precipitates.

Pyroxenes are the major host for iron in the lower, doleritic portion of the Red Hill intrusion, constituting between 40 and 50 % of the rock and containing ≈14–37 wt% FeO. They are strongly normally zoned in Fe–Mg, a trait that is characteristic of pyroxenes in the Tasmanian Dolerites (Hall et al. 1988). Iron in clinopyroxenes is hosted in the smaller M1 site, in octahedral co-ordination, favouring the preferential incorporation of ferrous over ferric iron (Carmichael and Ghiorso 1990; McCanta et al. 2004; Mallmann and O'Neill 2009). The $Fe^{3+}/\Sigma Fe_{px}$ varies with $Fe^{3+}/\Sigma Fe_{melt}$ (McCanta et al. 2004; Schoenberg et al. 2009) and exhibits lower ferric iron contents than the coexisting melts below ≈FMQ + 2 (McCanta et al. 2004; Mallmann and O'Neill 2009). The ideal stoichiometry of the pyroxenes, the ulvöspinel-rich composition of coexisting titanomagnetite (Hall et al. 1988), and the low $Fe^{3+}/\Sigma Fe$ content of the parental liquid (Fig. 5c) indicate oxygen-poor conditions within the magma chamber. As such, at equilibrium, the lighter isotopes of iron will preferentially enter the largely ferrous iron-containing pyroxenes as opposed to the melt.

Since there is a finite amount of oxygen available to the system, crystallisation of these Fe^{2+}-rich (and thus O_2-poor) phases diminishes the fraction of Fe^{2+} remaining in the liquid, resulting in a coupled increase in $Fe^{3+}/\Sigma Fe_{melt}$ (and therefore f_{O_2}) and $\delta^{57}Fe$. Magnetite stability is sensitive to the prevailing redox conditions (Toplis and Carroll 1995; Toplis and Carroll 1996), crystallising as function of the $Fe^{3+}/\Sigma Fe$ of the melt. The inflection in $\delta^{57}Fe$ in the Red Hill sequence at ≈1 wt% MgO marks a significant petrologic transition from pyroxenes to magnetite as the primary host of iron (Fig. 3). Due to the incorporation of Fe^{3+} in magnetite, $^{IV}(Fe^{3+})^{VI}(Fe^{3+} + Fe^{2+})_2O_4$, as compared to the predominantly Fe^{2+}-bearing pyroxenes, $^{VIII}Ca^{VI}(Mg,Fe^{2+})^{IV}Si_2O_6$, both total Fe and $Fe^{3+}/\Sigma Fe$ enrichment in the melt ceases (Fig. 5b, c). Magnetite (Mtn_{95}) in the Red Hill suite is saturated at the maximum f_{O_2}, in conjunction with fayalite, defining the FMQ buffer:

$$Fe_2SiO_4 + O_2 = Fe_3O_4 + SiO_2. \quad (3)$$

Therefore, at the apex of the $Fe^{3+}/\Sigma Fe$-$\delta^{57}Fe$ trend, the f_{O_2} of the melt is buffered. By analogy, the iron isotopic composition of the melt is also buffered, as dictated by the equilibrium exchange between fayalite and magnetite (Eq. 2; Shahar et al. 2008). The magnetite in the granophyric rocks is systematically enriched in the heavier isotopes compared to the pyroxenes with which it is in equilibrium (Fig. 6), a function of the relative concentrations of ferric iron in the two phases. When a_{FeO}^{liquid} becomes impoverished enough such that fayalite becomes exhausted, continued precipitation of magnetite then drives the f_{O_2} of the melt to lower values and concomitantly depletes it in ^{57}Fe.

Iron isotope composition of mineral phases

Owing to the high stratigraphic level of the intrusion, the instantaneous formation of chilled margins prevented not only wall-rock assimilation, but the escape of magmatic fluids from the system. Furthermore, the dearth of primary hydrous phases in the magmas, even in the differentiated granophyric rocks, suggests that the melt was poor in volatiles and not vapour-saturated (McDougall 1962). Therefore, the iron isotope variability in the Red Hill intrusion is most likely controlled by crystal-liquid processes. Analyses of the minerals that comprise the suite of magmatic rocks provide an ideal means by which to test this hypothesis.

The pyroxene–magnetite pairs in the fayalite granophyre (Mtn_{95}) and the granophyres ($Mtn_{95–85}$) lie on a line that defines a $\Delta^{57}Fe_{mtn-px} = +0.30\,‰$ (Fig. 6). Taking an average $\beta^{57/54}Fe_{px} = 0.5 \times 10^6/T^2$ (Polyakov and Mineev 2000) yields equilibration temperatures for these pyroxene–magnetite pairs of ≈900–1,000 °C. Such temperatures are in broad agreement with those recorded by the whole-rock compositional thermometer of Sisson and Grove (1993) (Table 1), indicating equilibrium existed between these minerals. Contrastingly, the two pyroxene–magnetite pairs from the dolerites define a trend perpendicular to the expected equilibrium line. Their $\Delta^{57}Fe_{mtn-px}$ are +0.77 and +0.51 ‰ for the dolerite 47 (≈Mtn_{40}) and the quartz dolerite 50 (≈Mtn_{70}), respectively. The corresponding temperatures, 550 and 750 °C, are not only drastically lower than would be expected for these magmas, but also in inverse correlation with their host bulk rock temperatures (≈1,150 and ≈1,100 °C, respectively, Table 1).

The pyroxenes in the doleritic series are unique in that they preserve very extensive normal Fe–Mg zoning, in contrast to the pyroxenes in the chilled dolerites, fayalite granophyres and the fayalite granophyres and granophyres, which are homogeneous (Fig. 2; McDougall 1962; Hall et al. 1988). The clear textural evidence for disequilibrium in these pyroxenes and their anomalously ^{57}Fe-depleted compositions is suggestive of kinetic processes. Recent experimental studies indicate that chemical diffusion between two phases can promote isotopic fractionation, owing to the faster diffusivity of the lighter isotope

(Roskosz et al. 2006; Richter et al. 2009a). The extent of kinetic isotope fractionation is proportional to the relative mass difference between the isotope pairing and is given by $\frac{D_2}{D_1} = \left(\frac{m_1}{m_2}\right)^{\gamma}$, where D_n corresponds to the diffusivity of isotope n and γ is a complex function of the medium of diffusion and the chemical characteristics of the element. While γ, and therefore differential diffusivity, typically decreases with increasing atomic mass (Richter et al. 2009b), Teng et al. (2011) found that δ^{57}Fe varied from +0.1 to −1.7 ‰ in olivines ranging from Fo_{80} to Fo_{84}, respectively, in a single bulk rock sample. The pyroxenes in the dolerites show a far wider range of Mg#s (Fig. 2b). However, because the whole of the pyroxene fraction was analysed, the extreme isotopic zones are homogenised, resulting in an average δ^{57}Fe which is ≈0.15 to 0.25 ‰ lighter than what might be expected based on an equilibrium pyroxene composition in the chilled dolerites. This may be ascribed to preferential diffusion of the lighter Fe isotopes into pyroxene during crystallisation in an attempt to equilibrate with the surrounding ^{57}Fe-enriched melt. The preservation of chemical zoning indicates that this process did not go to completion, resulting in zonation in Fe (and presumably Mg) isotope composition.

Crucially, the occurrences of magnetite in the doleritic rocks of Red Hill (samples 47 and 50) do not affect the liquid line of descent of the remaining melt—a decrease in Fe and Ti in the whole rocks is only observed following the crystallisation of Mtn_{95} in the fayalite granophyres. This, in conjunction with the interstitial nature of these oxides, implies that they crystallised from an intercumulus liquid. This liquid was necessarily Fe^{3+}-enriched due to the earlier crystallisation of pyroxenes and plagioclase and was therefore also likely to be enriched in δ^{57}Fe. The inordinate ^{57}Fe enrichment in these ulvöspinel-rich titanomagnetites is then a product of its closed-system crystallisation, which itself occurs within a system closed with respect to oxygen, rather than equilibrium between titanomagnetite and pyroxene.

Factors affecting the iron isotope composition of magmas during differentiation

The Rayleigh equation, which assumes perfect fractional crystallisation and is therefore an end-member scenario, is applied to model the observed isotopic fractionation in the whole rocks. In order to simplify the calculations, and taking into account the low $Fe^{3+}/\Sigma Fe$ of the chilled dolerites, both augite and pigeonite are assumed to incorporate negligible Fe^{3+} ($D^{Fe^{3+}}_{pyroxene-melt} = 0$) and, as such, have identical β-factors, while the iron hosted in plagioclase was ignored. Thus, ferrous and ferric iron were treated as two separate elements and modelled independently. Constraints on the cotectic proportions of the fractionating phases were estimated from least squares calculations, enabling estimation of the fraction of melt remaining (f) and making for an internally consistent dataset.

Stable isotope fractionation was also estimated using the Rayleigh equation:

$$\left(\frac{^{57}Fe}{^{54}Fe}\right)_{at\,f} = \left(\frac{^{57}Fe}{^{54}Fe}\right)_{original} f^{(\alpha_{prod-reac}-1)} \quad (4)$$

where f is the fraction of iron remaining in the melt normalised to its initial content. This equation is cast into delta notation and solved for the fractionation factor, α. The relative effect each phase has on determining α is scaled by multiplying its modal abundance by the concentration of iron (ferrous or ferric) in that phase. As the temperature has an important, but predictable effect on the magnitude of the isotopic fractionation, temperatures for the whole rocks were estimated according to Sisson and Grove (1993). The fraction of Fe remaining in the melt as a function of the original iron content is known from least squares calculations, making solving for α possible. The fractionation factors of the phases involved are iteratively adjusted until the model curve visually approximates that of the data (details in Online Resource C).

Early gabbroic fractionation in the Red Hill suite is modelled with a fractionation factor of $\Delta^{57}Fe_{px-melt} = -0.25\,‰ \times 10^6/T^2$, resulting in effective fractionation factors of −0.11 to −0.17 ‰ between pyroxene and melt at the magmatic temperatures inferred for the rocks (Table 1). Fractionation factors of $\Delta^{57}Fe_{mineral-melt} \approx -0.15\,‰$ were also found to account for the isotopic variation during differentiation of the Hekla magmas (Schuessler et al. 2009) and at Kilauea Iki (Teng et al. 2008). The equilibrium pyroxene-melt fractionation factor modelled is taken to be a maximum estimate, given the effect of kinetic processes (see "Iron isotope composition of mineral phases"). The decrease in δ^{57}Fe enacted by the crystallisation of cumulus magnetite in the granophyric rocks may be modelled using $\Delta^{57}Fe_{mtn-melt} = +0.20\,‰ \times 10^6/T^2$, resulting in effective $\Delta^{57}Fe_{mtn-melt} = +0.11 - +0.14\,‰$ at the calculated temperatures.

The veracity of these calculations can be tested by casting them against experimental values where the isotopic fractionation between predominantly Fe^{2+}-bearing silicates and magnetite has been defined. The β-factor for magnetite is well characterised based on nuclear inelastic resonant X-ray scattering synchrotron data to be $\beta^{57/54}Fe_{mtn} \approx 0.96 \times 10^6/T^2$ (Polyakov et al. 2007). However, the $\beta^{57/54}$ factors for Fe^{2+} silicates vary from $0.43 \times 10^6/T^2$ for the A site in Enstatite to $0.57 \times 10^6/T^2$ in olivine (Polyakov and Mineev 2000). Taking these as the minimum and maximum values for Fe^{2+}-bearing silicates,

the theoretical $\Delta^{57}Fe_{mtn-px}$ ranges from $+0.53$ ‰ $\times 10^6/T^2$ to $+0.39$ ‰ $\times 10^6/T^2$. The value of $\Delta^{57}Fe_{mtn-px} = +0.45\,‰ \times 10^6/T^2$ calculated in this study compares favourably with these estimates; however, it is considerably greater than $\Delta^{57}Fe_{mtn-fay} = +0.30\,‰ \times 10^6/T^2$ (Shahar et al. 2008) and the $\Delta^{57}Fe_{mtn-FeMgSil} = +0.25\,‰ \times 10^6/T^2$ of Valaas-Hyslop et al. (2008). The $\Delta^{57}Fe_{mtn-bt/amph}$ measured in differentiated siliceous magmas (Heimann et al. 2008) show a range of values from $+0.1$ to $+0.55$ ‰ at temperatures between 900 and 700 °C. While the absolute magnitude of isotopic fractionation between ferromagnesian silicates and magnetite varies substantially, it is notable that the fractionation factor derived in our model ($\Delta^{57}Fe_{mtn-px} = +0.45\,‰ \times 10^6/T^2$) predicts a $\Delta^{57}Fe_{mtn-px}$ of $+0.28$ and $+0.33$ ‰ at 1,000 and 900 °C, respectively. These numbers are in good agreement with the values obtained for the pyroxene–magnetite pairs in the fayalite granophyres and granophyres ($\approx +0.3$ ‰, Table 2), demonstrating that the model is internally consistent.

Implications

The effect of mineral composition: systems open and closed to oxygen exchange

The composition of Fe-bearing minerals can change as a function of f_{O_2}, most notably, the ilmenite–hematite and magnetite–ulvöspinel series (Buddington and Lindsley 1964). In common igneous minerals, β-factors vary with Fe^{2+}/Fe^{3+} (Polyakov and Mineev 2000) in the sequence $\beta_{Hem} > \beta_{Mtn} > \beta_{Ol,PX} > \beta_{Ilm}$. The difference in β-factors between the two end-members of the hematite–ilmenite series is $\Delta^{57}Fe_{hem-ilm} = +0.61\,‰ \times 10^6/T^2$, corresponding to $\approx +0.5$ ‰ at 800 °C, reflecting a change from 100 % Fe^{3+} to 100 % Fe^{2+} in VI-fold co-ordination. While no experimental or theoretical data exist for pure ulvöspinel, it is probable that an equivalent difference also occurs between magnetite and ulvöspinel. The magnetite–ulvöspinel solid solution is described by the formula $^{IV}\left(Fe^{3+}_{1-X}Fe^{2+}_{X}\right)^{VI}\left(Fe^{2+}Fe^{3+}_{1-X}Ti_X\right)O_4$, where magnetite corresponds to X = 0 and ulvöspinel to X = 1. In increasingly ulvöspinel-rich titanomagnetites, not only does the ferric iron content tend towards 0, but the bond lengths in the tetrahedral site increase to accommodate the larger Fe^{2+} ion (Bosi et al. 2009). The attendant decrease in the force constant of the bond should favour the accommodation of the lighter isotopes of Fe, assuming equilibrium conditions (e.g. Schauble 2004). Experimental quantification of the fractionation factor between magnetite and Fe^{2+}–Mg silicates shows, unequivocally, an enrichment in the heavier isotopes of iron in magnetite (Polyakov and Mineev 2000; Polyakov et al. 2007; Shahar et al. 2008). However, the experimentally derived fractionation factor between titanomagnetite and rhyolitic melt at 800 °C and 0.2 GPa yielded a negative $\Delta^{57}Fe_{mtn-melt} = -0.18\,‰$ (Schuessler et al. 2006). The fractionation factor determined in this study is relevant to almost pure magnetite, Mtn_{95}, and, based on the foregoing discussion, is almost certainly not applicable to titanomagnetite with a low Mtn content.

In addition to this work, iron isotope compositions for cogenetic magmas over a range of compositions are reported for two other tholeiitic systems: Hekla (Schuessler et al. 2009) and Kilauea Iki (Teng et al. 2008). When plotted against Mg#, the magmas from Red Hill and Kilauea Iki show immediate enrichment in $\delta^{57}Fe$ with decreasing Mg# (Fig. 7). Over the same interval, the lavas from Hekla show little variation in their isotopic composition before $\delta^{57}Fe$ increases drastically at Mg# = 20. Contrastingly, the Red Hill granophyres show a sudden drop in $\delta^{57}Fe$ at this stage of their evolution. The origins of the iron isotope variations in these tholeiitic suites are discussed below.

The Red Hill intrusion is subject to conditions closed to oxygen exchange. Early crystallisation of Fe^{3+}-poor phases (pyroxenes, Petrologic Evolution of the Red Hill suite, olivine at Kilauea) triggers an increase in the Fe^{3+} content of the remaining liquid because the O_2 budget is fixed. The tholeiitic magmas in this study, and that of Teng et al. (2008), reach a maximum in $\delta^{57}Fe$ at the inferred point of the Fe–Mg silicate to magnetite transition at Mg# = 20 (Fig. 7). Experimental studies show that the timing and composition of titanomagnetite along with magnetite–ulvöspinel solid solution series is dependent on the relative f_{O_2} of the melt (Toplis and Carroll 1995; Berndt et al. 2005; Botcharnikov et al. 2008; Feig et al. 2010). The precipitation of Mtn_{95} at Red Hill, implying relatively oxidising conditions at its saturation consistent with a build-up of Fe^{3+} in the melt, causes a dramatic decrease in the $\delta^{57}Fe$ of the remaining liquid thereafter.

In open igneous systems, the melt evolves along f_{O_2} trajectories defined by the amount of oxygen exchanged. Natural systems often evolve along paths where $Fe^{3+}/\Sigma Fe_{melt}$ parallels that of the FMQ buffer (Carmichael 1991; Toplis and Carroll 1996). In such a system, the $Fe^{3+}/\Sigma Fe$ of the magma reflects that of the crystallising phases, because $Fe^{3+}/\Sigma Fe_{melt}$ is fixed. Fe–Ti oxide analyses from a suite of magmatic rocks from Thingmuli, Iceland (Carmichael 1967), record f_{O_2}s that lie on the FMQ buffer, implying evolution open to oxygen exchange. Ilmenite–titanomagnetite pairs from basaltic andesites from the Hekla volcano (Baldridge et al. 1973) equilibrated at $\approx$1,050 °C at FMQ,

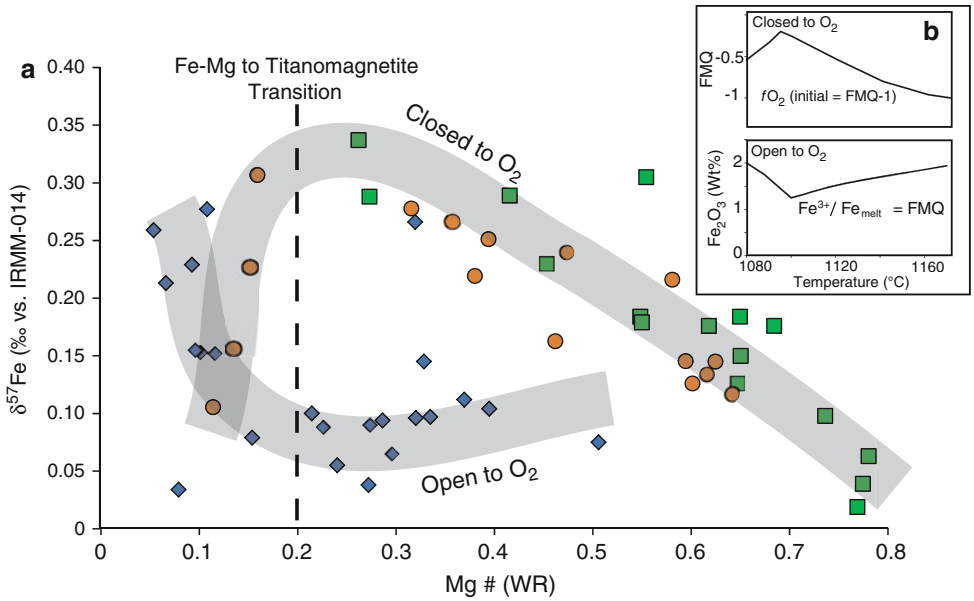

Fig. 7 δ^{57}Fe of whole rocks against their Mg#, characterising the change in iron isotope composition with differentiation. **a** Analyses of co-genetic whole-rock samples from tholeiitic suites: *green squares* = Kilauea Iki (Teng et al. 2008), *blue diamonds* = Hekla (Schuessler et al. 2009), *orange circles* = Red Hill (this study) display disparate behaviour depending on whether the system evolved *open* (Hekla) or *closed* (Red Hill, Kilauea Iki) to oxygen exchange (see Systems open and closed to oxygen exchange). **b** Simplified versions of Figs, 4 and 7 (Toplis and Carroll 1996), highlighting the contrasting change in $Fe^{3+}/\Sigma Fe_{WR}$ for conditions open and closed to oxygen exchange. These trends directly mirror those seen in **a**

falling on the T-f_{O_2} curve defined by the Thingmuli lavas, indicative of formation under similar redox conditions. Importantly, the composition of the crystallising titanomagnetite is $\approx Mtn_{35}$, in stark contrast to the Mtn_{95} that forms at Red Hill. To a first order, this is illustrative of a difference in the f_{O_2}, and therefore $Fe^{3+}/\Sigma Fe$, of the liquid from which the titanomagnetite crystallised. The titanomagnetite at Hekla, due to its low Fe^{3+} content, causes the increase in δ^{57}Fe observed in the siliceous differentiates, which climb from +0.08 ‰ at Mg# = 15 to +0.26 ‰ at Mg# = 6 (Schuessler et al. 2009; Fig. 7).

In fact, the Mg#–δ^{57}Fe evolution defined by magmas both closed and open with respect to oxygen mirrors that observed for temperature–ΔFMQ, Fe_2O_3 relations under the same conditions (Toplis and Carroll 1996, their Figs. 4, 7) (inset, Fig. 7b). Temperature varies as a linear function of the Mg# (Toplis and Carroll 1995) and may be used as a proxy for the degree of differentiation. The point of difference in Mg#-δ^{57}Fe systematics between the two systems is the $Fe^{3+}/\Sigma Fe$ of the melt. The ferric iron content of the melt is allowed to increase in closed systems, but stays constant in buffered systems. As a result, titanomagnetite crystallisation at FMQ, where its composition is closer to ulvöspinel, induces an increase in δ^{57}Fe in the melt (Schuessler et al. 2009). However, as shown for the first time here, it can dramatically lower δ^{57}Fe in the residual melt when it approximates end-member magnetite that crystallises from a more oxidised melt.

Application to granitic magmas

The iron isotope composition of granitic magmas ranges from δ^{57}Fe ≈ 0 ‰ up to ≈+0.6 ‰ (Poitrasson and Freydier 2005; Heimann et al. 2008). Evolving magmas that deviate markedly from the mafic igneous rock baseline of δ^{57}Fe ≈ 0.1 ‰ are generally restricted to SiO_2 contents >70 wt%, though exceptions to this are found in closed tholeiitic systems (Teng et al. 2008, this work). While differentiated, siliceous rocks tend towards more ^{57}Fe-enriched compositions, the cause of this shift remains unresolved. There are two prevailing schools of thought; that the change is achieved either by fractional crystallisation (Schoenberg and von Blanckenburg 2006; Teng et al. 2008; Schuessler et al. 2009) or through the exsolution of isotopically light, Fe^{2+}-bearing fluids (Poitrasson and Freydier 2005; Heimann et al. 2008).

Fluid exsolution

During the evolution of granitic magmas, dissolved water becomes less soluble as a result of the increasing polymerisation of the silicate framework in the melt (Holtz et al. 2001 and references therein), resulting in the saturation of a fluid phase during decompression. Such fluids have the capacity to complex metals, including iron, especially when rich in chloride. Fe^{2+} is the most soluble iron species, tending to co-ordinate itself with Cl^-, forming

$FeCl_2^0$ complexes (Chou and Eugster 1977). Calculations based on vibrational spectra on the $FeCl_4^-$ species (the closest analogue) indicate that the iron-bearing fluid should have significantly lighter Fe than its host granite (Schauble et al. 2001), as long as the remaining Fe is hosted in magnetite, defining a $\Delta^{57}Fe_{mtn-Fe^{2+}fluid} \approx +0.42‰ \times 10^6/T^2$ (Heimann et al. 2008). In this model, the iron isotope composition of granitic magmas is not directly tied to their differentiation history, but rather to the temperature and extent of iron loss in the fluid, and will therefore impact those granites with low residual Fe contents most strongly. Potential support for this phenomenon is provided by a decrease in Zr/Hf ratio with increasing δ^{57}Fe (Heimann et al. 2008). Because Zr and Hf exhibit similar crystal-melt coefficients, they are easily decoupled in fluids (Veksler 2004 and references therein), although Linnen and Keppler (2002) suggest fractional crystallisation of zircon can also account for this behaviour.

In order for exsolution to occur, the siliceous magma must be fluid-saturated at the time of crystallisation. However, many granites, most notably A-types (see below) are relatively dry and do not become saturated in a fluid phase (Clemens et al. 1986; Dall'agnol et al. 1999), as attested to by the lack of primary hydrous minerals in these rocks. The heaviest iron isotope compositions are restricted almost exclusively to A-type granitoids (Fig. 8), which could imply that these granites have lost the most Fe^{2+}-bearing fluid. The solubility of iron in the fluid phase is critically dependent on its Cl content and hence on $D^{Cl}_{Melt-Fluid}$. The Cl solubility shows a strong positive dependence on the molar (Na + K)/Al ratio of the melt (Métrich and Rutherford 1992). Many A-types are peralkaline and therefore have (Na + K)/Al ≥1, favouring the retention of Cl in the melt. A-type granites and rhyolites are characterised by low f_{O_2} assemblages where Fe^{2+} is stored in ferromagnesian silicates and oxides (ilmenite and titanomagnetite). In this case, exsolved fluid will not be in equilibrium with pure magnetite, but with Fe^{2+}-bearing oxides, significantly reducing the melt-fluid fractionation factor. As an example, the Coso rhyolites, in which (Na + K)/Al ≈ 1 and δ^{57}Fe ≈ 0.4 ‰ (Heimann et al. 2008), record f_{O_2} s = ΔFMQ − 0.5 (Bacon et al. 1981; Manley and Bacon 2000), identical to that of MORB (Bézos and Humler 2005).

The contention that Zr and Hf are only appreciably decoupled from one another by a fluid is belied by variations in Zr/Hf in MORB, caused by clinopyroxene fractionation (Jenner and O'Neill 2012) and zircon crystallisation in granites (Linnen and Keppler 2002; Lowery Claiborne et al. 2006). In fact, investigation of the global granite database (GEOROC; http://georoc.mpch-mainz.gwdg.de/georoc/) reveals a systematic decrease in Zr/Hf from the primitive mantle value of 36 at ≤70 wt% SiO_2 down to ≈15 at 78 wt% SiO_2, implying that it is a general characteristic of granitic magmas rather than attributable to fluid exsolution.

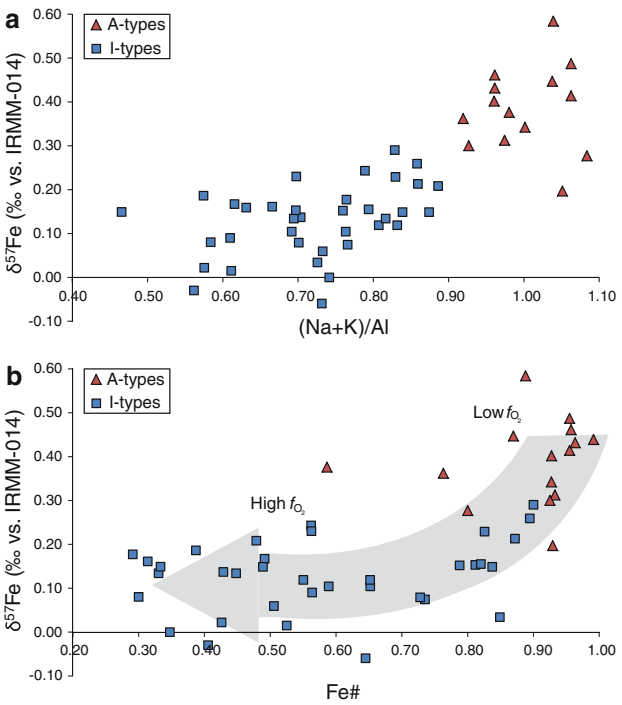

Fig. 8 Compilation of the δ^{57}Fe of evolved granitic whole-rock samples (intrusive and extrusive; SiO_2 ≥60 wt%) from the literature (Poitrasson and Freydier 2005; Poitrasson 2006; Schoenberg and von Blanckenburg 2006; Heimann et al. 2008; Dauphas et al. 2009; Schuessler et al. 2009; Craddock and Dauphas 2011) classified into A- and I-type granitoids (see Application to granitic magmas). **a** A- and I-type magmas define distinct populations where δ^{57}Fe varies with molar (Na + K)/Al. **b** I-type granitoids display uniformly low δ^{57}Fe at low Fe#, while A-types extend to ^{57}Fe-enriched and are typically ferroan. This illustrates that the increase in δ^{57}Fe with increasing Fe# is a function of the f_{O_2} of the magma

Fluid-mobile elements, such as Li, should be sensitive to the loss or ingress of deuteric fluids in the differentiating magma. In the cogenetic suite of magmatic rocks from Hekla (Schuessler et al. 2009), Li behaves as a moderately incompatible element, showing no evidence for depletion owing to the exsolution of a fluid phase. Moreover, δ^7Li remains constant over the course of magmatic differentiation, from SiO_2 = 52 to 73 wt%, while Fe isotopes increase from δ^{57}Fe = +0.08 to +0.26 ‰ (Schuessler et al. 2009; Fig. 7). The lack of Li isotope fractionation in evolving magmas is consistent with previous studies on basaltic rocks (Tomascak et al. 1999).

There are a variety of factors that can influence the extent of iron isotope fractionation caused by fluid exsolution. The first requirement, the presence of a free fluid phase, is fulfilled most frequently by metaluminous (I-type)

granitoids produced in arc environments, owing to their high water contents. These magmas crystallise at higher pressures and lower temperatures than A-types, favouring transport of iron in a chlorine-rich vapour (Simon et al. 2004). This evidence comes from melt inclusion data in phenocrysts in volcanic equivalents of these magmas (Wallace 2005 and references therein) which have elevated water contents with respect to tholeiitic magmas and their differentiates. This fluid phase is in equilibrium with early-formed Mtn-rich magnetite, maximising the $\Delta^{57}Fe_{mtn-Fe^{2+}fluid}$ fractionation factor. However, despite forming in conditions favourable for iron-rich fluid loss, I-type magmas exhibit consistently lighter δ^{57}Fe values compared with A-types (Fig. 8), suggesting that the iron isotope composition of siliceous magmas is primarily controlled by another process.

Fractional crystallisation

The alternative hypothesis, that the iron isotope composition of granitoids reflects the conditions of crystallisation, may be investigated by considering the chemistry of siliceous magmas. Based on the fundamental chemical differences between A- (low f_{O_2} and H_2O content) and I-type (high f_{O_2} and H_2O content) granites and their extrusive equivalents, it may be possible to track their histories via iron isotopes. In order to facilitate such a comparison, analyses of those granitoid rocks ($\geq$60 wt% SiO_2) with iron isotope analyses were compiled from the literature and chemically classified according to the scheme of Frost et al. (2001) into A-, I- and S-type granites (Online Resource D). Of the 67 for which major element chemical analyses were readily available, 15 fall into the A-type category and 36 into the I-type. A-type magmas have elevated (Na + K)/Al coupled with heavy δ^{57}Fe (avg. = +0.39 ± 0.06 ‰), clearly separate from their I-type counterparts (Fig. 8a). Similarly, in a plot of Fe# (ΣFe/(ΣFe + Mg)) versus δ^{57}Fe (Fig. 8b), the I-types generally show low Fe# at low δ^{57}Fe (avg. = +0.13 ± 0.05 ‰), whereas the A-types are distinctly ferroan and have universally high δ^{57}Fe values.

Qualitatively, these characteristics can be explained by equilibrium Fe isotope partitioning between the crystallising phases and melt. The magmas parental to I-type granitoids—subduction-related high-Al basalts and andesites, crystallise olivine, which is then succeeded by plagioclase, two pyroxenes (augite and orthopyroxene) and magnetite (Grove and Juster 1989; Sisson and Grove 1993). Importantly, due to their high f_{O_2} and H_2O contents (e.g. Whalen and Chappell 1988), Mtn-rich magnetite is saturated early in the crystallisation sequence, causing iron depletion in the remaining melt, such that MgO and $Fe_2O_3^{(T)}$ decrease at similar rates, keeping Mg# near constant. The crystallisation of ^{57}Fe-depleted, Fe^{2+}-phases (ferromagnesian silicates) and ^{57}Fe-enriched, Fe^{3+}-bearing phases (magnetite) effectively buffers the Fe isotope composition of the melt such that it remains close to its original value. The I-type differentiates, which crystallise amphibole, biotite and magnetite as their Fe-bearing phases, therefore have reasonably low δ^{57}Fe at low Fe#s. For example, the siliceous I-type magmas from Questa (Johnson et al. 1989) have f_{O_2}s half-way between FMQ and hematite–magnetite (which, at 800 °C, corresponds to FMQ + 2.5) and typically correspondingly low δ^{57}Fe, averaging +0.17 ± 0.07 ‰. Only the peralkaline, high-silica magmas (e.g. sample 82-QC-32C, Heimann et al. 2008) exhibit high δ^{57}Fe, up to +0.45 ‰.

A-type granites show evidence for protracted fractional crystallisation in their highly enriched incompatible trace element abundances and pronounced negative Eu anomalies (e.g. Turner et al. 1992; Namur et al. 2011) and major element compositions that closely approximate the ternary granite eutectic minimum (Tuttle and Bowen 1958; Ebadi and Johannes 1991). Dry A-type magmas, characterised by their low f_{O_2} (Turner et al. 1992; Frost and Frost 1997; Frost and Frost 2011; Namur et al. 2011), have their iron hosted in ferromagnesian silicates (e.g. hedenbergite, fayalite) and oxides (Mtn-poor titanomagnetite and ilmenite), all of which contain dominantly Fe^{2+} and are ^{57}Fe-depleted (Polyakov and Mineev 2000). By crystallising such minerals, ^{57}Fe-, alkali-enriched A-type residual melts with high Fe# form. Additionally, alkalis, inversely proportional to their ionisation potential, stabilise Fe^{3+}, in tetrahedral co-ordination (Dickenson and Hess 1986; Farges et al. 2004; Mysen and Richet 2005; Bingham et al. 2007), augmenting the affinity of heavy iron for the melt. Examples of ^{57}Fe-enriched A-type granites include NSL (peralkaline rhyolite from New Zealand, δ^{57}Fe = +0.44 ‰; Schoenberg and von Blanckenburg 2006) and the peralkaline aegirine-, arfvedsonite-bearing granite EV9101 from Evisa, Corsica, δ^{57}Fe = +0.58 ‰; Poitrasson and Freydier 2005).

The recognition that A- and I-type granites define two distinct populations in their iron isotope composition lends credence to the petrographic and chemical evidence which suggests their derivation from reduced and oxidised parent magmas, respectively. The fact that iron isotopes correlate with indices of magmatic differentiation has been recognised in numerous works (e.g. Teng et al. 2008). Combining this knowledge with theoretical and experimental partitioning mechanics of iron isotopes between different mineral phases (e.g. Polyakov and Mineev 2000; Shahar et al. 2008), which demonstrate that heavier isotopes show a greater affinity for phases that incorporate ferric iron, it becomes apparent that magmas which crystallise different

minerals will preserve different iron isotope compositions. As calc-alkaline magmas are found only in subduction zone settings, the light (δ^{57}Fe $\approx +0.13 \pm 0.05$ ‰, Fig. 8) iron isotope composition of the resultant I-type granitoids is therefore indicative of formation in an oxidising environment. Conversely, A-type magmas crystallise phases stabilised under reducing conditions and low H_2O contents, traits characteristic of tholeiitic magmas. These magmas are derived from mantle that was unaffected by subduction zone fingerprints and are found in intraplate environments (continental flood basalts, MORB and some OIBs). Thus, iron isotopes are able to act as a reliable proxy for the oxidation state, and therefore, the tectonic settings, of evolved granitic rocks.

Conclusion

The pronounced effect crystal fractionation imparts on the $Fe^{3+}/\Sigma Fe$ of melts during igneous differentiation controls the evolution of the isotopic composition of iron. We have demonstrated that the iron isotope composition of a tholeiitic melt closed to oxygen exchange will become heavier due to removal of early-fractionating pyroxenes which deplete the melt in Fe^{2+}, and enrich it in Fe^{3+}. In the latter stages of differentiation, when f_{O_2} is sufficiently high, magnetite becomes the dominant iron-bearing phase and sequesters Fe^{3+} and isotopically enriched iron. Calculated mineral-melt iron isotope fractionation factors show that VI-fold co-ordinated Fe^{2+}-pyroxenes are lighter than coexisting melt ($\Delta^{57}Fe_{px-melt} = -0.25\,‰ \times 10^6/T^2$), whereas magnetite's high $Fe^{3+}/\Sigma Fe$ and partly tetrahedrally co-ordinated Fe^{3+} make it a suitable host for the heavier isotopes of iron ($\Delta^{57}Fe_{mtn-melt} = +0.20\,‰ \times 10^6/T^2$). Such partitioning mechanics are confirmed by pyroxene–magnetite pairs, which, at equilibrium, define a $\Delta^{57}Fe_{mtn-px} = +0.30\,‰$ at 900–1,000 °C in the granophyric rocks. In the dolerites, pyroxene–magnetite disequilibrium results from diffusion-controlled isotope fractionation in zoned pyroxenes, and the late crystallisation of titanomagnetite from the intercumulus liquid. The equilibrium partitioning systematics of Fe isotopes point to an intimate link between the isotopic composition and the oxygen fugacity of the melt, which affects the valence and hence structural state of iron between phases. Iron isotopes therefore act as effective probes of the redox state and tectonic settings of terrestrial magmas.

Acknowledgments We are indebted to John Stanley for performing the XRF analyses, and Jason Kirby and Claire Wright at the CSIRO for their assistance with the daily running of the MC-ICP-MS. Oliver Nebel, Adriana Heimann and two anonymous reviewers are greatly thanked for their constructive and in-depth reviews. We particularly appreciate the insightful comments and editorial handling of Franck Poitrasson that significantly improved the manuscript.

References

Bacon CR, Macdonald R, Smith RL, Baedecker PA (1981) Pleistocene high-silica rhyolites of the Coso volcanic field, Inyo County, California. J Geophys Res 86(11):10223–10241

Baldridge WS, McGetchin TR, Frey FA, Jarosewich E (1973) Magmatic evolution of Hekla, Iceland. Contrib Miner Petrol 42:245–258

Beard BL, Johnson CM, Skulan JL, Nealson KH, Cox L, Sun H (2003) Application of Fe isotopes to tracing the geochemical and biological cycling of Fe. Chem Geol 195(1–4):87–117

Berndt J, Koepke J, Holtz F (2005) An Experimental Investigation of the Influence of water and oxygen fugacity on differentiation of MORB at 200 MPa. J Petrol 46(1):135–167

Bézos A, Humler E (2005) The $Fe^{3+}/\Sigma Fe$ ratios of MORB glasses and their implications for mantle melting. Geochim Cosmochim Acta 69(3):711–725

Bingham P, Parker JM, Searle TM, Smith I (2007) Local structure and medium range ordering of tetrahedrally coordinated Fe^{3+} ions in alkali–alkaline earth–silica glasses. J Non-Cryst Solids 353(24–25):2479–2494

Bosi F, Halenius U, Skogby H (2009) Crystal chemistry of the magnetite-ulvöspinel series. Am Miner 94:181–189

Botcharnikov RE, Almeev RR, Koepke J, Holtz F (2008) Phase relations and liquid lines of descent in hydrous ferrobasalt-implications for the Skaergaard intrusion and Columbia River flood basalts. J Petrol 49(9):1687–1727

Buddington AF, Lindsley DH (1964) Iron-titanium oxide minerals and synthetic equivalents. J Petrol 5:310–357

Campbell IH, Nolan J (1974) Factors effecting the stability field of Ca-poor pyroxene and the origin of the Ca-poor minimum in Ca-rich pyroxenes from tholeiitic intrusions. Contrib Miner Petrol 48:205–219

Carmichael ISE (1967) The mineralogy of Thingmuli, a Tertiary volcano in eastern Iceland. Am Min 52:1815–1841

Carmichael ISE (1991) The redox states of basic and silicic magmas: a reflection of their source regions? Contrib Miner Petrol 106:129–141

Carmichael ISE, Ghiorso MS (1990) The effect of oxygen fugacity on the redox state of natural liquids and their crystallizing phases. In Nicholls J, Russell JK (eds) Modern Methods of igneous petrology: understanding magmatic processes, vol. 24. Mineralogical Society of America Reviews in Mineralogy, pp 191–212

Chou I-M, Eugster HP (1977) Solubility of magnetite in supercritical chloride solutions. Am J Sci 277:1296–1314

Clemens JD, Holloway JR, White AJR (1986) Origin of A-type granites: experimental constraints. Am Min 71:317–324

Craddock PR, Dauphas N (2011) Iron isotopic compositions of geological reference materials and chondrites. Geostand Geoanal Res 35(1):101–123

Dall'agnol R, Scaillet B, Pichavant M (1999) An experimental study of a Lower Proterozoic A-type granite from the eastern Amazonian craton, Brazil. J Petrol 40(11):1673–1698

Dauphas N, Craddock PR, Asimow PD, Bennett VC, Nutman AP, Ohnenstetter D (2009) Iron isotopes may reveal the redox conditions of mantle melting from Archean to Present. Earth Planet Sci Lett 288(1–2):255–267

Dickenson MP, Hess PC (1986) Contributions to mineralogy and the structural role and homogeneous redox equilibria of iron in

peraluminous, metaluminous and peralkaline silicate melts. Contrib Miner Petrol 92:207–217
Ebadi A, Johannes W (1991) Beginning of melting and composition of first melts in the system Qz-Ab-Or-H_2O-CO_2. Contrib Miner Petrol 106:286–295
Encarnaciòn J, Fleming TH, Elliot DH, Eales HV (1996) Synchronous emplacement of Ferrar and Karoo dolerites and the early breakup of Gondwana. Geology 24:535–538
Farges F, Lefrère Y, Rossano S, Berthereau A, Calas G, Brown GE Jr (2004) The effect of redox state on the local structural environment of iron in silicate glasses: a combined XAFS spectroscopy, molecular dynamics, and bond valence study. J Non-Cryst Solids 344(3):176–188
Feig ST, Koepke J, Snow JE (2010) Effect of oxygen fugacity and water on phase equilibria of a hydrous tholeiitic basalt. Contrib Miner Petrol 160(4):551–568
Fenner CN (1929) The crystallization of basalts. Am J Sci 5(18):225–253
Foden JD, Elburg MA, Dougherty-Page JS, Burt A (2006) The timing and duration of the Delamerian orogeny: correlation with the Ross Orogen and implications for Gondwana assembly. J Geol 114(2):189–210
Frost CD, Frost BR (1997) Reduced rapakivi-type granites: the tholeiite connection. Geology 25(7):647–650
Frost CD, Frost BR (2011) On ferroan (A-type) granitoids: their compositional variability and modes of origin. J Petrol 52(1):39–53
Frost BR, Barnes CG, Collins WJ, Arculus RJ, Ellis DJ, Frost CD (2001) A geochemical classification for granitic rocks. J Petrol 42(11):2033–2048
Grove TL, Juster TC (1989) Experimental investigations of low-Ca pyroxene stability and olivine-pyroxene-liquid equilibria at 1-atm in natural basaltic and andesitic liquids. Contrib Miner Petrol 103(3):287–305
Hall RP, Hughes DJ, Joyner L (1988) Fe-enrichment in tholeiitic pyroxenes: complex two-pyroxene assemblages in Mesozoic dolerites, southern Tasmania. Geol Mag 125(6):573–582
Heimann A, Beard BL, Johnson CM (2008) The role of volatile exsolution and sub-solidus fluid-rock interactions in producing high 56Fe-54Fe ratios in siliceous igneous rocks. Geochim Cosmochim Acta 72:4379–4396
Hergt JM, Chappell BW, McCulloch MT, McDougall I, Chivas AR (1989) Geochemical and isotopic constraints on the origin of the Jurassic dolerites of Tasmania. J Petrol 30:841–883
Holtz F, Johannes W, Tamic N, Behrens H (2001) Maximum and minimum water contents of granitic melts generated in the crust: a re-evaluation and implications. Lithos 56(1):1–14
Jayasuriya KD, O'Neill HSC, Berry AJ, Campbell SJ (2004) A Mössbauer study of the oxidation state of Fe in silicate melts. Am Miner 89:1597–1609
Jenner FE, O'Neill HSC (2012) Analysis of 60 Elements in 616 ocean floor basaltic glasses. Geochem Geophys Geosyst. doi:10.1029/2011GC004009
Johnson CM, Czamanske GK, Lipman PW (1989) Geochemistry of intrusive rocks associated with the Latir volcanic field, New Mexico, and contrasts between evolution of volcanic and plutonic rocks. Contrib Miner Petrol 103:90–109
Linnen RL, Keppler H (2002) Melt composition control of Zr/Hf fractionation in magmatic processes. Geochim Cosmochim Acta 66(18):3293–3301
Lowery Claiborne L, Miller CF, Walker BA, Wooden JL, Mazdab FK, Bea F (2006) Tracking magmatic processes through Zr/Hf ratios in rocks and Hf and Ti zoning in zircons: an example from the Spirit Mountain batholith, Nevada. Miner Mag 70(5):517–543
Mallmann G, O'Neill HSC (2009) The crystal/melt partitioning of V during mantle melting as a function of oxygen fugacity compared with some other elements (Al, P, Ca, Sc, Ti, Cr, Fe, Ga, Y, Zr and Nb). J Petrol 50(9):1765–1794
Manley CR, Bacon CR (2000) Rhyolite thermobarometry and the shallowing of the magma reservoir, Coso volcanic field, California. J Petrol 41(1):149–174
McCanta MC, Darby-Dyar M, Rutherford MJ, Delany JS (2004) Iron partitioning between basaltic melts and clinopyroxene as a function of oxygen fugacity. AmMiner 89:1685–1693
McDougall I (1962) Differentiation of the Tasmanian dolerites: Red Hill dolerite-granophyre association. Geol Soc Am Bull 73:279–316
Métrich N, Rutherford MJ (1992) Experimental study of chlorine behavior in hydrous silicic melts. Geochim Cosmochim Acta 56(2):607–616
Mysen BO, Richet P (2005) Developments in geochemistry: vol. 10—silicate glasses and melts—properties and structure. Elsevier, B.V, Amsterdam, p 544
Namur O, Charlier B, Toplis MJ, Higgins MD, Hounsell V, Liégeois J-P, Vander Auwera J (2011) Differentiation of tholeiitic basalt to A-type granite in the Sept Iles layered intrusion, Canada. J Petrol 52(3):487–539
Osborn EF (1959) Role of oxygen pressure in the crystallization and differentiation of basaltic magma. Am J Sci 257:609–647
Papike JJ, Karner JM, Shearer CK (2005) Comparative planetary mineralogy: valence state partitioning of Cr, Fe, Ti, and V among crystallographic sites in olivine, pyroxene, and spinel from planetary basalts. Am Miner 90(2–3):277–290
Poitrasson F (2006) On the iron isotope homogeneity level of the continental crust. Chem Geol 235:195–200
Poitrasson F, Freydier R (2005) Heavy iron isotope composition of granites determined by high resolution MC-ICP-MS. Chem Geol 222(1–2):132–147
Polyakov VB, Mineev SD (2000) The use of Mössbauer spectroscopy in stable isotope geochemistry. Geochim Cosmochim Acta 64(5):849–865
Polyakov VB, Clayton RN, Horita J, Mineev SD (2007) Equilibrium iron isotope fractionation factors of minerals: re-evaluation from the data of nuclear inelastic resonant X-ray scattering and Mössbauer spectroscopy. Geochim Cosmochim Acta 71:3833–3846
Richter FM, Dauphas N, Teng F-Z (2009a) Non-traditional fractionation of non-traditional isotopes: evaporation, chemical diffusion and Soret diffusion. Chem Geol 258:92–103
Richter FM, Watson EB, Mendybaev RA, Dauphas N, Georg RB, Watkins J, Valley JW (2009b) Isotopic fractionation of the major elements of molten basalt by chemical and thermal diffusion. Geochim Cosmochim Acta 73:4250–4263
Roskosz M, Luais B, Watson HC, Toplis MJ, Alexander CMOD, Mysen BO (2006) Experimental quantification of the fractionation of Fe isotopes during metal segregation from a silicate liquid. Earth Planet Sci Lett 248:851–867
Schauble EA (2004) Applying stable isotope fractionation theory to new systems. In: Johnson CM, Beard BL, Albarede F (eds) Geochemistry of non-traditional stable isotopes. Mineralogical Society of America, Washington, DC, pp 65–111
Schauble EA, Rossman GR, Taylor HP Jr (2001) Theoretical estimates of equilibrium Fe-isotope fractionations from vibrational spectroscopy. Geochim Cosmochim Acta 65(15):2487–2497
Schmidt PW, McDougall I (1977) Palaeomagnetic and potassium-argon dating studies of the Tasmanian Dolerites. Aust J Earth Sci 24(5–6):321–328
Schoenberg R, von Blanckenburg F (2006) Modes of planetary-scale Fe isotope fractionation. Earth Planet Sci Lett 252(3–4):342–359
Schoenberg R, Marks MAW, Schuessler JA, von Blanckenburg F, Markl G (2009) Fe isotope systematics of coexisting amphibole

and pyroxene in the alkaline igneous rock suite of the Ilímaussaq Complex, South Greenland. Chem Geol 258(1–2):65–77

Schuessler JA, Schoenberg R, Behrens H, von Blanckenburg F (2006) Quantification of iron isotope fractionation between sulphide and oxide minerals and silicate melts. American Geophysical Union (AGU) Fall Meeting Abstract: V21B-0574

Schuessler J, Schoenberg R, Sigmarsson O (2009) Iron and lithium isotope systematics of the Hekla volcano, Iceland—evidence for Fe isotope fractionation during magma differentiation. Chem Geol 258:78–91

Shahar A, Young ED, Manning CE (2008) Equilibrium high-temperature Fe isotope fractionation between fayalite and magnetite: an experimental calibration. Earth Planet Sci Lett 268:330–338

Simon AC, Pettke T, Candela PA, Piccoli PM, Heinrich CA (2004) Magnetite solubility and iron transport in magmatic-hydrothermal environments. Geochim Cosmochim Acta 68(23):4905–4914

Sisson TW, Grove TL (1993) Temperatures and H_2O contents of low-MgO high-alumina basalts. Contrib Miner Petrol 113(2):167–184

Snyder D, Carmichael ISE, Wiebe RA (1993) Experimental study of liquid evolution in an Fe-rich, layered mafic intrusion: constrains of Fe-Ti oxide precipitation on the T-fO_2 and T-ρ paths of tholeiitic magmas. Contrib Miner Petrol 113:73–86

Taylor PDP, Maeck R, De Bièvre P (1992) Determination of the absolute isotopic composition and atomic weight of a reference sample of natural iron. Int J Mass Spectrom Ion Proc 121(1–2): 111–125

Teng F-Z, Wadhwa M, Helz RT (2007) Investigation of magnesium isotope fractionation during basalt differentiation: implications for a chondritic composition of the terrestrial mantle. Earth Planet Sci Lett 261(1–2):84–92

Teng F-Z, Dauphas N, Helz RT (2008) Iron isotope fractionation in Kilauea Iki Lava Lake. Science 320:1620–1622

Teng F-Z, Dauphas N, Helz RT, Gao S, Huang S (2011) Diffusion-driven magnesium and iron isotope fractionation in Hawaiian olivine. Earth Planet Sci Lett 308(3–4):317–324

Tomascak PB, Tera F, Helz RT, Walker RJ (1999) The absence of lithium isotope fractionation during basalt differentiation: new measurements by multicollector sector ICP-MS. Geochim Cosmochim Acta 63(6):907–910

Toplis MJ, Carroll MR (1995) An experimental study of the influence of oxygen fugacity on Fe-Ti oxide stability, phase relations, and mineral-melt equilibria in ferro-basaltic systems. J Petrol 36(5):1137–1170

Toplis MJ, Carroll MR (1996) Differentiation of ferro-basaltic magmas under conditions open and closed to oxygen: implications for the Skaergaard Intrusion and other natural systems. J Petrol 37:837–858

Turner SP, Foden JD, Morrison RS (1992) Derivation of some A-type magmas by fractionation of basaltic magma: an example from the Padthaway Ridge, South Australia. Lithos 28:151–179

Tuttle OF, Bowen NL (1958) Origin of granite in the light of experimental studies in the system $NaAlSi_3O_8$-$KAlSi_3O_8$-SiO_2-H_2O. Geol Soc Am Mem 74:153

Valaas-Hyslop E, Valley JW, Johnson CM, Beard BL (2008) The effects of metamorphism on O and Fe isotope compositions in the Biwabik Iron Formation, northern Minnesota. Contrib Miner Petrol 155:313–328

Veksler IV (2004) Liquid immiscibility and its role at the magmatic-hydrothermal transition: a summary of experimental studies. Chem Geol 210(1–4):7–31

Wallace PJ (2005) Volatiles in subduction zone magmas: concentrations and fluxes based on melt inclusion and volcanic gas data. J Volcanol Geoth Res 140:217–240

Whalen JB, Chappell BW (1988) Opaque mineralogy and mafic mineral chemistry of I- and S-type granites of the Lachlan foldbelt, southeast Australia. Am Miner 73:281–296

Williams IS, Hergt JM (2000) U–Pb dating of Tasmanian dolerites: a cautionary tale of SHRIMP analysis of high-U zircon. In: Woodhead JD, Hergt JM, Noble WP (eds) Beyond 2000: new frontiers in isotope geoscience. School of Earth Sciences, University of Melbourne, Melbourne, pp 185–188

Wilson AD (1960) The Microdetermination of ferrous iron in silicate minerals by a volumetric and a colorimetric method. Analyst 85:823–827